Identifying Moving Groups Using Elemental Abundances – A Study of KFR08

Petter Thorén

Lund Observatory
Lund University

2011-EXA56

Degree project of 15 higher education credits
August 2011

Lund Observatory
Box 43
SE-221 00 Lund
Sweden

Abstract

In this work we study nine Hipparcos stars that has been identified as members of the KFR08 stellar stream by Bobylev et al. (2010). We perform high-resolution elemental abundance analysis on these stars using spectra from several sources (ELODIE, HIRES, MIKE and UVES) and the abundance analysis method from Bensby et al. (2003). Furthermore, we perform an angular momentum analysis of the stars using methodology from Kepley et al. (2007) and make an age estimation using Hipparcos photometry and Bertelli et al. (2009) isochrones.

We find that five out of nine stars are members of a possible KFR08 moving group with metallicity [Fe/H]$\simeq -0.90$ dex and an age of roughly 12 Gyrs. However, a small sample size makes the identification of a KFR08 moving group uncertain.

Populärvetenskaplig beskrivning

När man studerar stjärnors rörelse så talar man ofta om så kallade stjärnströmmar (jfr engelska *stellar streams*). Dessa stjärnströmmar består av ett antal stjärnor som har liknande hastigheter, dvs. stjärnor som i stort rör sig tillsammans. Dessa strömmar kan bildas på lite olika sätt. T.ex. så kan en dvärggalax fångas in av Vintergatan. När detta sker så kommer tidvattenkrafter att slita sönder den mindre galaxen så att den lämnar efter sig ett band av stjärnor i sin omloppsbana. Dessa stjärnor kommer ha hastigheter som liknar de som deras modergalax hade, och man kan på så sätt urskilja dem från andra stjärnor. Det finns också en speciell grupp av strömmar, kända som rörelsegrupper (jfr engelska *moving groups*). Dessa grupper av stjärnor har precis som andra stjärnströmmar egenskapen att de har liknande hastigheter men skiljer sig från de i att de är födda ur ett och samma gasmoln. Detta faktum gör att rörelsegruppernas stjörnor har samma kemiska sammansättning samt att de är lika gamla.

I detta examensarbete studerar vi nio stjärnor ur strömmen KFR08, en grupp med stjärnor som 2008 identifierades som en stjärnström. Vi gör en detaljerad grundämnesanalys av våra nio stjärnor, samt tittar på deras rörelsemängdsmoment och ålder. Vi gör detta i syfte att se ifall KFR08 möjligen kan vara en rörelsegrupp. Vi finner tecken på att fem av de nio stjärnor vi studerat kan vara medlemmar i en rörelsegrupp, men på grund av att det är så få stjärnor vi studerat så är det omöjligt att säga med säkerhet.

1 Introduction

In this project we aim to use chemical elemental abundances to determine whether a group of stars identified as kinematically similar in the literature are members of a single stellar population or not. To do this, we perform a stellar abundance analysis to study the metallicities and elemental abundances of the stars. We also look at the angular momenta and ages of the stars to determine if they are members of the same stellar population or not.

This first section contains an overview of the Milky Way, moving groups and halo streams. The second section describes the abundance analysis. In the third section we present our results, and in the fourth section we discuss the implications of the results and look towards the future in this field of study. Finally, appendix A lists all data from the abundance analysis.

1.1 The Milky Way

Our galaxy, the Milky Way, is made up of three main stellar components; the bulge, the disk and the halo. Out of these, the halo has, by far, the largest extent with a radius of $\sim$50 kpc and a spheroidal shape. The Galactic disk is made up of two distinct components; the thin and the thick disk, both having a radius of $\sim$25 kpc (Buser 2000) but with differing thicknesses. Since the thin and thick disks are not sharply defined distributions of stars it is difficult to assign thicknesses to them. Instead, a so called scale height is used to define the thickness of each disk. The scale height is defined by fitting a stellar density function to one of the disks where the stellar density decreases exponentially outwards. The scale height, then, is the distance over which the stellar density decreases by a factor e. Determining a scale height of the thick and thin disks is done in, e.g., Jurić et al. (2008), where the scale heights of the disks are found to be $\sim$0.3 kpc for the thin disk and $\sim$0.9 kpc for the thick disk. The Galactic bulge in the centre of the Milky Way is very difficult to study. Because of the high dust density near the Galactic centre, observations are limited to the infra-red and radio wavelength regions. Today there is a general consensus that the bulge also includes some kind of elongated bar-like shape, but more precise dimensions and its angle in relation to the Earth are still actively debated. See Merrifield (2004) for a review of the Galactic bulge and Churchwell et al. (2009) (especially section 4.1) for a shorter and more recent summary.

Finally, there is a fourth, non-stellar component of the Milky Way; a

dark matter halo. Due to its dark matter nature, it can not be observed directly but is inferred mainly by looking at the rotation curve of the Milky Way. The rotation curve is the velocities of stars or gas in orbit around the Galactic centre plotted against their distance from the Galactic centre. In the Milky Way rotation curve, one sees that outside the bulge, the orbital velocity of objects remains almost constant regardless of distance from the Galactic centre. This contradicts what Kepler's laws and Newtonian mechanics predict (given that light traces mass, as it does for stars and gas), namely that orbital velocity decreases as $\sqrt{1/r}$ with increasing distance, r, from the Galactic centre. This discrepancy is attributed to a very large, unseen, mass outside the bulge, containing a majority of the Milky Way's total mass. The most likely candidate for this mass is a large dark matter halo.

1.1.1 The Milky Way Disk

In spiral galaxies, such as the Milky Way, the Galactic disk has a clear spiral structure, which is made up of the spiral arms. The arms are the most gas-rich parts of the galaxy, and is therefore where most new star formation takes place. Because of this they house a relatively higher proportion of young stars. One should not believe that the space between the spiral arms is empty, it is merely less luminous due to the fact that it contains fewer young, very bright, stars.

Since the spiral arms contain a large amount of gas, they can be mapped by studying HII regions (clouds of ionized hydrogen), the vast majority of which are located in the spiral arms. Despite this, the complex structure of the spiral arms is not well understood (see Hou et al. 2009, for a recent attempt at mapping the spiral arms).

To understand the evolution and structure of the Milky Way, it is important to carefully trace its evolution far back in time. For the halo this can be done using globular clusters which are very old and tightly bound (and therefore stable) systems. In the Galactic disk, on the other hand, there are very few globular clusters so one has to study the less tightly bound open clusters. Most open star clusters will dissipate into the stellar background over a timescale of $\sim 10^8$ years (Spitzer 1958) which makes it difficult to trace the evolution of the disk longer than that far back in time.

1.2 A Note on Coordinate Systems

In this report we use a rectangular coordinate system centred on the observer with the X-axis directed away from the Galactic centre, the Y-axis in the direction of the Galactic rotation and the Z-axis directed towards the North Galactic Pole. The U, V and W components of an object's space velocity are directed along the respective axes. Note that positive U-velocities are directed *away from* the Galactic centre, along the X-axis. Furthermore, all velocities are given relative to the local standard of rest.

The local standard of rest (LSR) is a concept that enables us to study the true motion of stars relative to the Sun more easily. Since all stars in the Milky Way orbit the Galactic centre, they will on average have a large V-velocity. The LSR is this velocity in the solar neighbourhood. According to Binney & Merrifield (1998) the local standard of rest is "the current velocity of a fictional particle that moves around the plane of the Milky Way on the closed orbit in the plane that passes through the present location of the Sun." They also note that "If the Milky Way is axisymmetric, this orbit is circular, otherwise it is oval." The LSR tells you what velocity the matter in a small volume around the Sun has on average. The IAU has adopted a standard value for v_{LSR} =220 km s^{-1} which is what we use in this report. Since the LSR is not explicitly the Sun's velocity in its orbit around the Galactic centre, the Sun will have a motion relative to the LSR. This motion can be measured by studying the average motion of stars and assuming them to have random velocity distributions. This has been done by, e.g., Dehnen & Binney (1998) whose motion of the Sun relative to the LSR, $[u_\odot, v_\odot, w_\odot] = [-10.00, 5.23, 7.17]$ km s^{-1}, we use in this report.

1.3 Moving Groups

The concept of moving stellar groups was first introduced by Olin Eggen in the 1960's. Originally Eggen defined a moving group as a number of stars with a common V-velocity. The idea is that the stars in the group form from a common gas cloud orbiting the Galaxy. The stars in the group will have similar velocities, with small random internal velocities for the individual stars. These individual velocities will make the group, over several Galactic orbits, stretch into a tube-like structure around the Galaxy and finally disperse into the background of the Galactic disk. As such, moving groups provide a probe into eras of Galactic evolution older than those that

open clusters can provide. Because they eventually disperse, the moving groups are also the intermediate stage between cluster and field stars, and it is therefore of vital importance that we study and understand these systems if we are to unravel the evolution of the Milky Way.

Since the stars in a moving group form from a common gas cloud they should have similar metallicities and ages in addition to their shared spatial velocity. This property of the moving groups can be used as a membership criterion, just like velocities. Finding group members by their chemical abundances has the advantage over velocities in that chemical abundances will be preserved in dwarf stars, while their velocities can change due to gravitational interactions with other objects. In this way, it should be possible to map and understand the early period of our Galaxy's formation in order to get a better understanding of the galaxy formation process. This "chemical tagging" approach was first put forward by Freeman & Bland-Hawthorn (2002) with the long term goal of being able to identify individual progenitor gas clouds involved in the formation of the Galactic disk.

Not all groups of stars with similar velocities are moving groups, however. The Hercules stream, for example, was recently studied by Bensby et al. (2007) who found that, due to the large difference in ages and metallicities of the member stars, they can not stem from a single stellar population. Instead, they propose that the Hercules stream is a mixture of thin and thick disk stars which have had their kinematics altered by the Galactic bar so that they have similar velocities. The fact that not all kinematically similar groups of stars are distinct stellar populations means that the chemical tagging technique becomes very important in determining which groups of stars are true moving groups and which are not.

To date only one true moving group has been identified, known as HR 1614. HR 1614 was initially proposed as a moving group by Eggen (1978). He defined the HR 1614 moving group as the stars with a V-velocity within ± 10 km s^{-1} of the star HR 1614's V-velocity. Follow-up studies (e.g., Smith 1983) showed that many of Eggen's original member stars actually did not belong to the group. It remained difficult to reliably find member stars of HR 1614 due to the lack of good parallaxes until the Hipparcos data remedied this in 1997. The definite confirmation of HR 1614's existence came when Feltzing & Holmberg (2000) performed a study of the group using Hipparcos parallaxes and Strömgren photometry. They found that the HR 1614 group is about 2 Gyrs old, and has a super-solar metallicity [Fe/H] $\simeq 0.19$ dex. Their study also provided a sample of stars that are probable members of HR 1614. This

sample of stars (along with some of Eggen's stars) was then used by De Silva et al. (2007) to conduct a high-resolution abundance study of the HR 1614 moving group. They found the group to have a somewhat higher metallicity than what Feltzing & Holmberg (2000) did, at a mean [Fe/H]= 0.25. They also found four stars to be deviating in metallicity and could disqualify three of them from membership of the group after they had been found to either be spectroscopic binaries or having newly measured velocities placing them outside the main V-velocity clump as defined by Feltzing & Holmberg (2000). The fourth deviating star could not be disqualified, however, and De Silva et al. (2007) considers it plausible that this star lies in the kinematic and photometric intervals of the HR1614 group by pure chance. Disregarding these deviating stars, HR 1614 was found to have very low intrinsic scatter in its elemental abundances. This clear chemical homogeneity along with a clear similarity in age made De Silva et al. (2007) advocate that HR 1614 is in fact a true moving group, the dispersed remnants of an old star formation event.

1.4 Halo Streams

Halo streams are, as their name implies, found in the Galactic halo. Halo streams are kinematically similar to moving groups, i.e. both of them have member stars with similar V-velocities. Halo streams can differ from moving groups in their origin, however. Where moving groups are remnants of a star forming region that has dispersed over time, halo streams are remnants of dwarf galaxies or stellar clusters accreted by the Milky Way. This accretion process is very lengthy, and will over a long time make the progenitor system stretch into a stream-like structure along its orbit. Numerical simulations (e.g., Helmi et al. 2003) have shown that such stream structures can survive for several billions of years. When looking at elemental abundances, streams differ from moving groups in that their member stars are not necessarily chemically homogeneous or of the same age.

1.5 The KFR08 Stream

The KFR08 stream is a relatively recently discovered group of stars with similar positions in velocity space. The stream was discovered by Klement et al. (2008) using radial velocities from the first data release from the RAVE survey (Steinmetz et al. 2006) and proper motions from other major catalogues

(Starnet 2.0, Tycho-2, SuperCOSMOS, USNO-B, DENIS and 2MASS). Klement et al. (2008) searched for streams in the projection of velocity space spanned by $(U^2+2V^2)^{1/2}$ and V. In this plane, stars that have similar orbital eccentricity should form clumps, assuming an axisymmetric Galactic potential and that stars in the same stellar stream stay in orbits close together. With this method they found several well-documented streams and also the stream that came to be named KFR08 (see Fig. 1). Their location of the KFR08 stream in their velocity plane is $(V, \sqrt{U^2+2V^2}) \approx (-160, 220)$ km s^{-1}.

KFR08 was then studied by Bobylev et al. (2010) who presented a list of 19 Hipparcos stars that they considered probable members of the stream based on kinematic membership criteria. They found that the KFR08 stream is centred at $(V, \sqrt{U^2+2V^2}) = (-159, 227)$ km s^{-1} in velocity space and includes stars in a radius of 30 km s^{-1} around this centre. The member stars are distributed all over the sky but share common V-velocities, which can be seen in Table 1 where the velocities for each star are given. Bobylev et al. (2010) did not perform any abundance analysis of their own, but took metallicity values from the literature (see their article, Table 2 for a list of papers) where available. According to their paper, the KFR08 stream stars have [Fe/H] abundances ranging from -0.36 to -1.31 dex. They also obtained an isochrone age estimate of the stream of 13 Gyrs by comparing all their 19 stars to one isochrone and looking at the turnoff.

2 Elemental Abundance Analysis

The elemental abundance analysis was a standard abundance analysis, performed by Thomas Bensby using equivalent widths measured by the author. For a thorough explanation of the methods of the abundance analysis, see Bensby et al. (2003). The abundance analysis also included age estimation using isochrone fitting of the stars. A full list of all resulting element abundances can be found in Appendix A.

2.1 Selection of Objects

Stars to study were selected from Table 2 in Bobylev et al. (2010). From this table nine out of 19 proposed members of the KFR08 stream were selected for further study based on the availability of suitable stellar spectra in the

Table 1: This table lists the velocities of the stars that Bobylev et al. (2010) listed as probable members of KFR08. Stars listed first (above the line) are the stars that we study in this report. All velocities are given in km s^{-1}, relative to the local standard of rest. Note that the U-velocities are opposite to the ones in Bobylev et al. (2010) since our coordinate system has its X-axis directed in the opposite direction compared to theirs.

Star ID	$U_{LSR} \pm e_U$ km s^{-1}	$V_{LSR} \pm e_V$ km s^{-1}	$W_{LSR} \pm e_W$ km s^{-1}
HIP 5336	32±1	-153±1	-28±1
HIP 54469	-91±5	-159±16	-64±16
HIP 58357	123±16	-134±23	45±1
HIP 58708	14±3	-160±4	15±1
HIP 58843	-122±9	-138±14	-58±7
HIP 60747	-110±7	-146±14	91±7
HIP 74033	113±10	-132±10	42±7
HIP 81170	77±2	-157±9	-123±3
HIP 87101	76±5	-159±18	-3±2
HIP 15495	-58±4	-174±8	-3±3
HIP 18235	16±3	-161±4	-19±2
HIP 19143	140±3	-143±11	-42±2
HIP 55988	-50±4	-154±6	-25±4
HIP 59785	117±9	-136±6	-109±7
HIP 64920	-66±5	-159±5	43±5
HIP 93269	-70±3	-140±1	-4±3
HIP 93623	-130±5	-149±16	-20±1
HIP 96185	56±1	-156±1	-66±1
HIP 117702	-12±7	-159±7	124±5

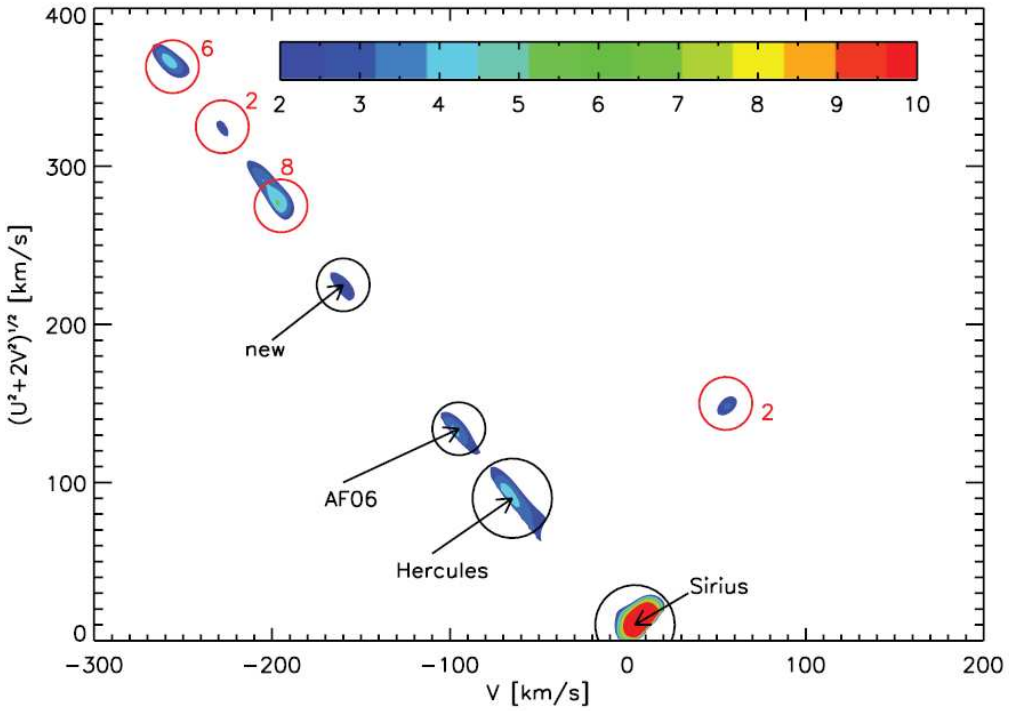

Figure 1: From Klement et al. (2008), this plot is where KFR08 (marked "new") was first discovered. The colours represent significance, with redder colour meaning more likely to be a stellar stream. For details, see sect. 1.5 and the Klement et al. (2008) article.

Table 2: This table lists all our stars and those from Bobylev et al. (2010), with both Hipparcos ID and an alternate ID. It also lists the coordinates for each star, taken from SIMBAD.

HIP ID	Alt. ID	RA (Deg)	Dec (Deg)
HIP 5336	* 30 Cas	017.06831127	+54.92034067
HIP 54469	LTT 4103	167.16697024	–44.25937121
HIP 58357	G 198-7	179.50033592	+48.20345558
HIP 58708	LHS2498	180.62048501	+43.08408433
HIP 58843	LHS 2507	181.02317462	+03.34075646
HIP 60747	G 13-38	186.74942627	+01.56622309
HIP 74033	HD 134113	226.94375025	+08.87978175
HIP 81170	HD 149414	248.67647458	–04.22907558
HIP 87101	G 154-21	266.94198236	–09.60512536
HIP 15495	LHS 1533	049.91605075	+33.59865559
HIP 18235	LTT 1823	058.49776976	–23.13707260
HIP 19143	LHS 187	061.54900065	+32.95086201
HIP 55988	LHS 305	172.11561474	+07.51727417
HIP 59785	LTT 4607	183.87687540	–41.91327762
HIP 64920	HD 115577	199.59755292	–28.33251990
HIP 93269	G 260-14	284.98995758	+64.05380906
HIP 93623	LHS 3427	285.98629657	–20.46015741
HIP 96185	LHS 3469	293.36283865	+33.20186565
HIP 117702	LHS 4031	358.06011982	–61.42515190

archives. Coordinates and alternative ID's for the nine selected stars, as well as for the rest of the Bobylev et al. (2010) sample are shown in Table 2.

Several archives were searched for high resolution spectra. The ELODIE archive, the ESO archive (UVES) and the Keck telescope archive (HIRES). We also had our own (not taken for this project) observations from the MIKE spectrograph on the Magellan telescopes in Las Campanas, Chile. In total, we found high-resolution spectra for nine stars. Of these, two were observed with ELODIE, two with HIRES, three with MIKE, and one with UVES. Which instrument each star was observed with is shown in Table 3.

2.2 Data

Our most important data are the spectra of our nine Hipparcos stars, which are the main sources of information to calculate metallicities. However, we also use parallaxes from the new Hipparcos reduction (van Leeuwen 2007) and *V*-magnitudes from the Hipparcos catalogue (ESA 1997) to determine the iron abundances. The parallaxes and magnitudes are used, along with effective temperatures and stellar masses, to calculate the surface gravity of a star. The Effective temperatures are determined by requiring iron lines with different excitation potentials to generate the same abundances. Furthermore, stellar mass is estimated using evolutionary tracks in an HR-diagram using stellar magnitudes and effective temperatures. Lastly, these quantities are used to construct model atmospheres which are used to derive abundances with measured equivalent line widths (see Bensby et al. 2003, for further elaboration).

Due to the fact that our spectra come from different instruments they have varying wavelength ranges, signal-to-noise ratios and normalization (all these parameters for each spectrum are listed in Table 3). This means that it is difficult to make equally good measurements for all stars. The HIRES spectra proved especially difficult to measure since they had very bad fringing and other anomalies in the extreme red end of the spectrum, making lines that fall there impossible to measure (see Fig. 2 for an example).

2.3 Equivalent Width Measurements

The **splot** task in the IRAF software package was used to measure spectral line equivalent widths of a number of elements and ions. We measured equivalent widths for all nine of our stars and a reference spectrum of the Sun to normalize the measurements against. Normalization was done on a line-to-line basis. Measuring the Sun's spectrum instead of using a set of standard solar equivalent widths is a way to reduce systematic measurement errors due to different measurement methods. The elements and ions we measured are: Na, Mg, Al, Si, Ca, Ti, TiII, Cr, CrII, Fe, FeII Ni, Zn, YII and BaII (for all elements without ionization levels indicated, only the abundance of neutral atoms was measured). The individual lines were taken from a list of 498 lines in the interval 4500-9000Å taken from Bensby et. al (in prep.), although not every line was possible to measure in every star due to the low metallicity of some of them. Another limiting factor was that most of the

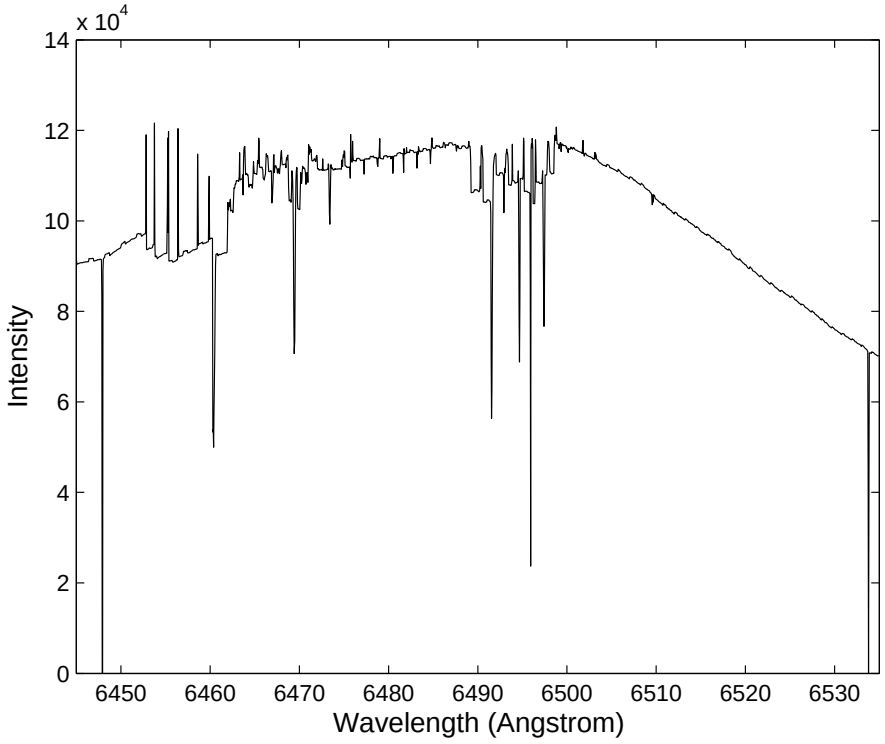

Figure 2: Example of anomalies in the HIRES spectra. This is aperture 26 of the HIP 81170 spectrum. Very bad anomalies make the majority of the aperture impossible to measure lines in.

Table 3: This table lists the wavelength range and signal-to-noise ratio (measured at 6045 Å) of the spectra used to measure abundances in our stars. It also lists what type of spectrum each was, whether it was normalized or not and the instrument with which the spectrum was taken.

Star ID	λ range (Å)	S/N	Spectrum source	Norm.	Instrument
HIP 5336	4000-6800	230	Continuous	No	ELODIE
HIP 54469	4860-8930	310	Continuous	Yes	MIKE
HIP 58357	4000-6800	240	Continuous	No	ELODIE
HIP 58708	3500-6190	30	Apertures (36)	No	HIRES
HIP 58843	4860-8930	300	Continuous	Yes	MIKE
HIP 60747	3800-6260	50	Apertures (37)	No	HIRES
HIP 74033	3300-6620*	370	Three parts	Yes	UVES
HIP 81170	4440-6870	150	Apertures (29)**	No	HIRES
HIP 87101	4860-8940	220	Continuous	Yes	MIKE

* Small parts (4500-4600 and 5600-5700) were missing in the gaps between the three spectrum parts.
** There were 29 apertures in this spectrum but apertures 26 - 29 were unusable due to anomalies in the spectrum.

stellar spectra did not provide data all the way to 9000Å, which made it impossible to measure some lines. See Table 3 for a complete list of spectral ranges for all our stars.

2.4 Post-measurement Cleanup

After the initial measurements had been made, the results were reviewed. Spectral lines in a star that were found to have generated abundances that were significantly deviating from the median abundance for that star were revisited and checked for errors in the measurement. HIP 5336 in particular had many lines very far from the median, which prompted us to remeasure all lines in its spectrum.

Figure 3 shows a comparison between our equivalent widths and measurements from Bensby et al. (in prep.). The plot is the difference between our and the Bensby et al. (in prep.) results as a function of wavelength. In Fig. 3 we see that there were problems with the equivalent width measurements at both ends of the spectra. These problems lead us to remove all measured lines at wavelengths shorter than 5075Å and longer than 8000Å from all our stars. A single Mg line at 8736.019Å was kept, however, since more than half of the 11 Mg lines in the list were above 8000Å and the one that was kept is the strongest Mg line in the list. Also in In Fig. 3, we can see that our equivalent widths are sytematically a little lower than those from Bensby et al. (in prep.). This is probably a systematic difference in the way we put the continuum when measuring lines, and is largely remedied by the measurement of the reference spectrum of the Sun.

2.5 Errors in the Abundances

We've used standard error analysis in this report. The notation below is taken from Gray (1992) where a small collection of formulae for error analysis can be found. The standard deviation, σ, listed in the tables in Appendix A is given by

$$\sigma = \sqrt{\frac{\sum (x_i - \bar{x})^2}{N-1}}$$

Where x_i is the abundance from line i, $\bar{x}$ is the mean abundance for the star and N is the number of lines of an element used for the abundance analysis

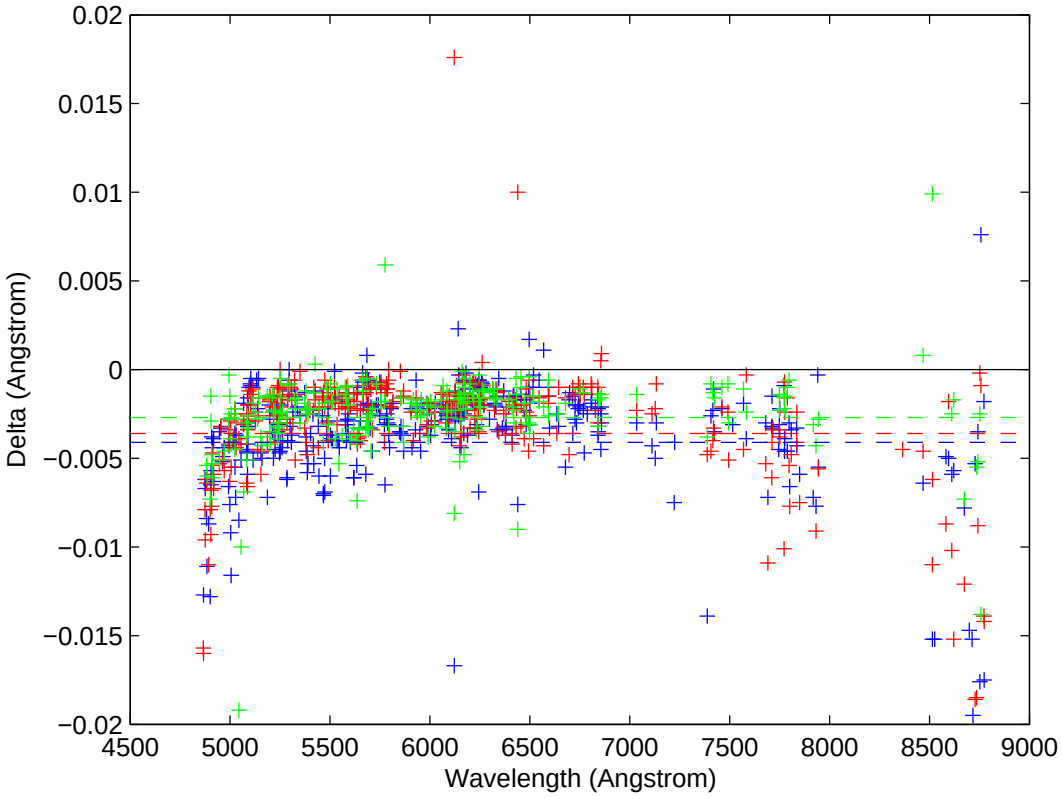

Figure 3: This figure shows our results compared to measured equivalent widths from Bensby et al. (in prep.) for the three stars that our studies have in common: HIP 54469 (blue crosses), HIP 58843 (red crosses) and HIP 87101 (green crosses). Delta represents the Bensby et al. results minus ours. We have also indicated mean equivalent width delta values for each star by the coloured dashed lines.

of that element. The error bars in the abundance plots (e.g., Fig. 4) are the errors in the mean abundance, given by

$$\bar{\sigma} = \frac{\sigma}{\sqrt{N}}$$

The[X/H] and [X/Fe] value of a star is given by

$$[X/H] = \log_{10}\left(\frac{N_X}{N_H}\right)_{Star} - \log_{10}\left(\frac{N_X}{N_H}\right)_{\odot}$$

$$[X/Fe] = \left[\log_{10}\left(\frac{N_X}{N_H}\right)_{Star} - \log_{10}\left(\frac{N_X}{N_H}\right)_{\odot}\right] - \left[\log_{10}\left(\frac{N_{Fe}}{N_H}\right)_{Star} - \log_{10}\left(\frac{N_{Fe}}{N_H}\right)_{\odot}\right]$$

Where N_X is the number of relevant atoms or ions per unit volume and N_H is the number of hydrogen atoms per unit volume. Furthermore, the error in [X/Fe], $\bar{\sigma}_{[X/Fe]}$ is given by

$$\bar{\sigma}_{[X/Fe]} = \sqrt{\bar{\sigma}_X^2 + \bar{\sigma}_{Fe}^2}$$

Assuming that there are no errors in the solar N_X values.

As can be seen in the tables in Appendix A, most abundances have rather large σ, not infrequently up to 0.3 dex. The reason for this is that we have quite a few lines giving strange abundance values, which is reflected both in the abundances and in the standard deviation, σ, of the abundances. When looking at $\bar{\sigma}$, the errors become smaller, however. Some of these lines would most likely have to be remeasured, had this been a larger project, but as it stands, remeasuring the anomalous lines is outside the scope of this project.

3 Results

In addition to the elemental abundances in Appendix A the abundance analysis yielded several other stellar parameters, listed in Table 4.

3.1 Metallicities

From Table 4 we can see that we have a group of stars with clearly similar metallicities in our nine stars. We have five stars within 0.1 dex of [Fe/H]= -0.90, (HIP 58357, HIP 58843, HIP 60747, HIP 74033 and HIP 81170) these

Table 4: This table lists the stellar parameters that resulted from the abundance analysis. The first column lists the effective temperature in Kelvin, the second lists the surface gravity, the third lists the micro-turbulence in km s^{-1}, the fourth lists the mass in solar masses, and the fifth to seventh columns list age estimates, from the abundance analysis, in Gyrs.

Star ID	[Fe/H]	$T_{\rm eff}$ (K)	$\log g$ ($\log$(cm s^{-2}))	ξ_t (km s^{-1})	Mass ($M_\odot$)	Age (Gyrs)	Age, low (Gyrs)	Age, high (Gyrs)
HIP 5336	-0.74	5505	4.59	0.20	0.80	-	-	-
HIP 54469	-0.52	5957	4.42	0.58	1.00	4.0	0.1	7.5
HIP 58357	-0.83	5435	3.51	1.17	1.42	2.5	1.8	3.1
HIP 58708	-0.33	5218	3.57	0.95	1.45	2.8	2.6	3.1
HIP 58843	-0.90	5642	4.31	0.36	0.78	12.7	10.0	15.0
HIP 60747	-0.85	5517	4.66	0.20	0.80	-	-	-
HIP 74033	-0.90	5725	3.99	1.04	0.88	12.1	10.2	13.6
HIP 81170	-0.93	5741	4.80	0.20	0.70	-	-	-
HIP 87101	-1.58	5664	4.06	0.43	0.70	22.5	17.5	24.0

stars will henceforth be referred to as the "main group". We also see that we have two clearly deviating stars in HIP 58708 and HIP 87101. HIP 54469 also has a high metallicity relative to the main group along with HIP 5336. HIP 5336 and HIP 54469, however, do not have high enough metallicities to be dismissed outright.

3.2 α-element Abundances

We can see from Fig. 4 that all our stars have high α-abundances. All stars have values above zero for all α elements except HIP 58357 which has [TiII/Fe]$= -0.27$ and HIP 81170 with [Si/Fe]$= -0.05$. Notable is also that our main group of stars at [Fe/H]$= -0.90$ have quite similar α abundances, especially the [Ca/Fe] values are very similar. The [Ti/Fe] values for the same stars are rather spread out, however, possibly due to larger errors.

3.3 Iron-peak Element Abundances

The iron-peak element abundances should lie close to the abundances for iron itself for all iron-peak elements, meaning that [X/Fe] should be zero on

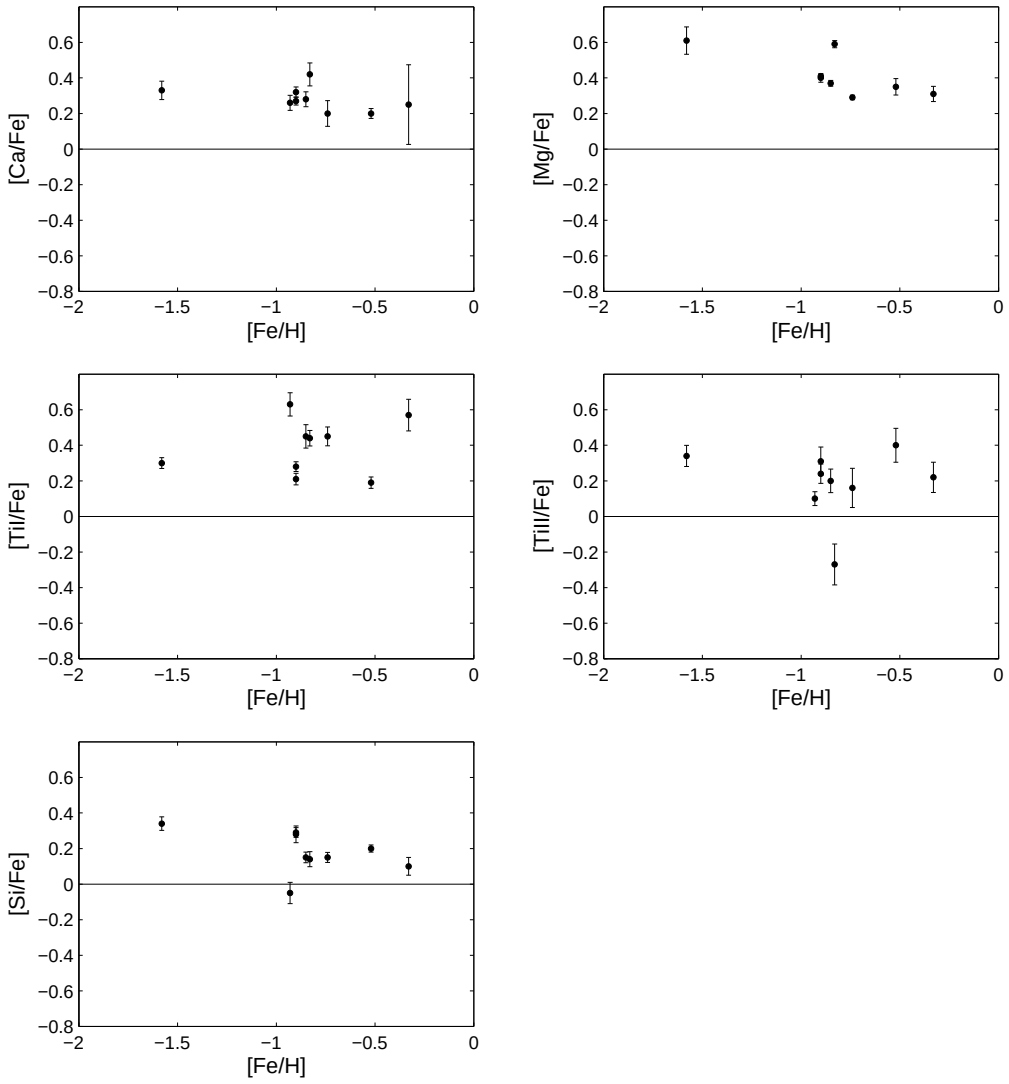

Figure 4: These five plots shows the abundance trends of Ca, Mg, Ti, TiII and Si in our stars. $\bar{\sigma}_{[X/Fe]}$ is indicated by vertical errorbars on each of the points.

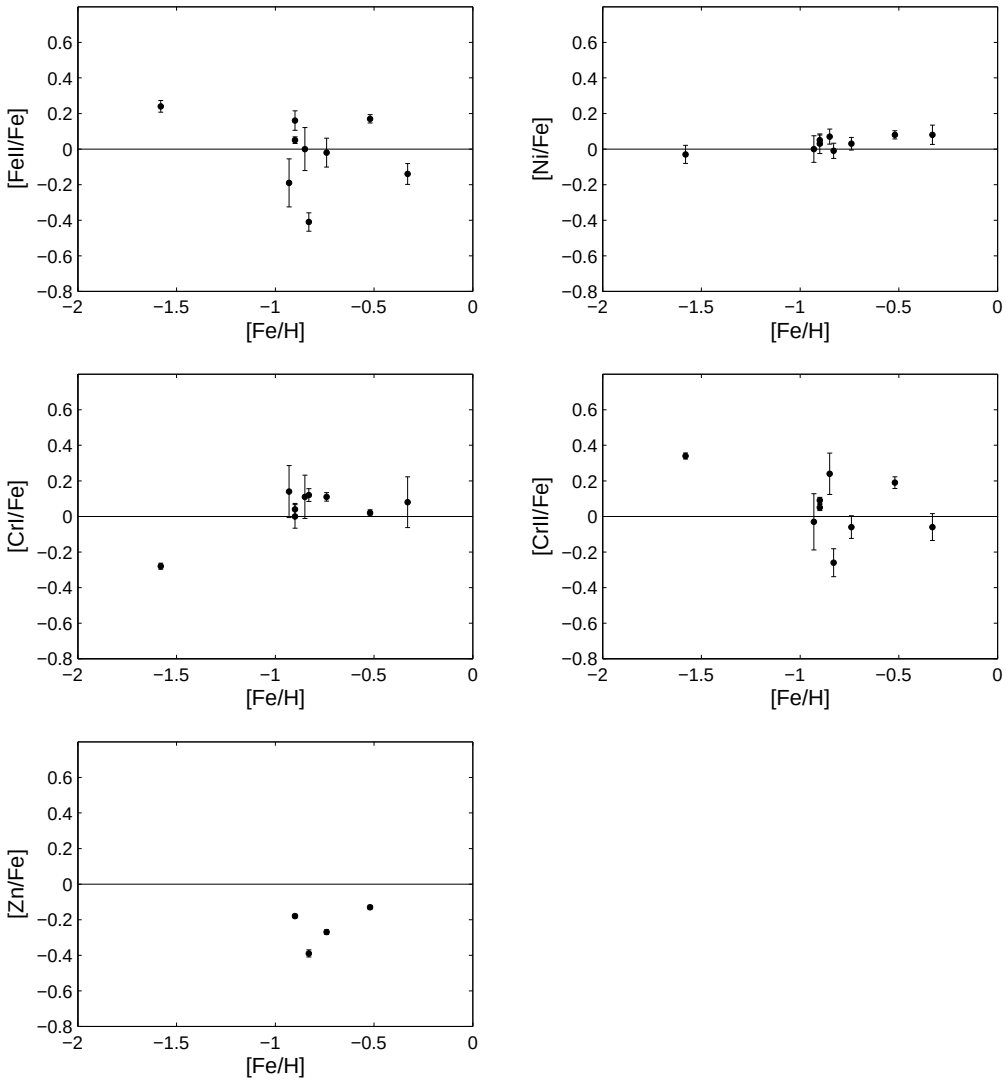

Figure 5: These five plots shows the abundance trends of FeII, Ni, Cr, CrI and Zn in our stars. $\bar{\sigma}_{[X/Fe]}$ is indicated by vertical errorbars on each of the points.

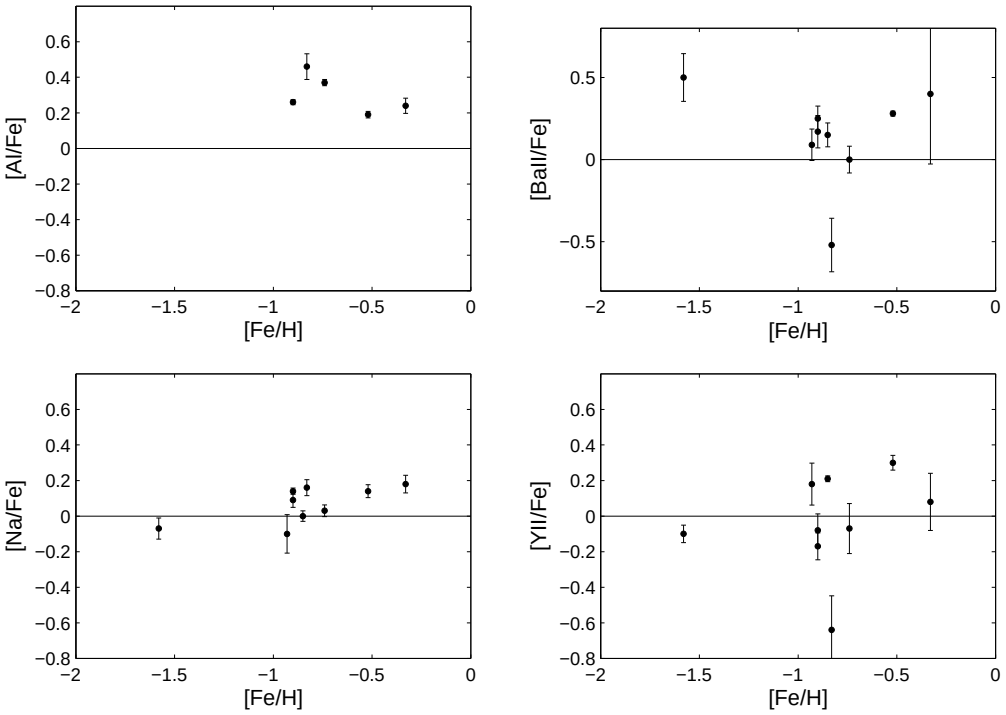

Figure 6: These four plots shows the abundance trends of Al, BaII, Na and YII in our stars. $\bar{\sigma}_{[X/Fe]}$ is indicated by vertical errorbars on each of the points.

average for iron-peak elements. As can be seen from Fig. 5 our stars have, on average, [Cr/Fe] abundances slightly above zero. The [Ni/Fe] values lie nicely around zero, though. We also have a large spread in our [FeII/Fe] plot. The strange abundance values in the [Zn/Fe] plot might be explained by the fact that there was only one Zn-line in our line list. This line was not possible to measure in five of our stars.

3.4 Al, Ba, Na and Y Abundances

As can be seen in Fig. 6 all of these elemental abundances, except [Na/Fe], show large scatter for all our stars. However, they all have very few measured lines, no element has more than five lines used to determine its abundance, which might contribute to the large spread. Most difficult to measure was

Al since all expect one weak Al line lie at wavelengths longer than 6600 Å, a wavelength range several of our spectra lack. It was impossible to measure the Al abundance for four out of nine stars. The Na abundances have less scatter and smaller errors than the rest of these elements. This might be due to that the few Na-lines measured are relatively strong (most Na lines have equivalent widths in excess of 50 mÅ, while most lines of other elements have equivalent widths between 10 and 30 mÅ) and easy to measure. This, however, makes them more susceptible to errors in the micro-turbulence.

3.5 Angular Momentum Analysis

We want to be able to determine the origin of old populations of stars that have been spatially mixed with the Milky Way's disc and halo. This becomes possible when looking at the angular momenta of stars, which are stable over a star's entire lifetime (Morrison et al. 2009). This means, e.g., that stars from galaxies accreted by the Milky Way will have different angular momenta from those in the disk or the halo.

The methodology below is taken from Kepley et al. (2007) and the notation is the same. To calculate the angular momentum of a star, we need to find its coordinates in a rectangular galactocentric coordinate system. Thus we first need to transform the Galactic coordinates of each star from a spherical coordinate system to a rectangular one.

$$
\begin{aligned}
x' &= -d\ cos(b)\, cos(l) \\
y' &= d\ cos(b)\, sin(l) \\
z' &= d\ cos(b)
\end{aligned}
$$

Where d is the distance to the star from the observer and b and l are the Galactic latitude and longitude, respectively. Now we have a rectangular coordinate system centred on the Sun, $[x', y', z']$, which we will need to translate so that it is centred on the Galactic centre. The distance from the Sun to the Galactic centre is 8 kpc, which means that our galactocentric coordinate system becomes

$$x = x' + 8kpc$$
$$y = y'$$
$$z = z'$$

Now, for the stellar velocities, one has to take into account the velocity of the LSR, and the Sun's velocity relative to the LSR. Thus,

$$v_x = U + u_\odot$$
$$v_y = V + v_\odot + v_{LSR}$$
$$v_z = W + w_\odot$$

For the velocity of the Sun relative to the LSR, we use the values from Dehnen & Binney (1998), $[u_\odot, v_\odot, w_\odot] = [-10.00, 5.23, 7.17]$ km s^{-1}. The velocity of the LSR, $v_{LSR} = 220$ km s^{-1}. Finally, the components of the angular momentum are given by the cross-products:

$$J_x = yv_z - v_y z \tag{1}$$
$$J_y = zv_x - v_z x \tag{2}$$
$$J_z = xv_y - v_x y \tag{3}$$

Angular momentum space is then plotted with $J_{Plane} = (J_x^2 + J_y^2)^{1/2}$ as a function of J_Z.

The errors in J_x J_y and J_z are given by.

$$\sigma^2_{J_x} = (yv_z)^2 \left(\left(\frac{\sigma_{v_z}}{v_z} \right)^2 + \left(\frac{\sigma_y}{y} \right)^2 \right) + (v_y z)^2 \left(\left(\frac{\sigma_{v_y}}{v_y} \right)^2 + \left(\frac{\sigma_z}{z} \right)^2 \right)$$

$$\sigma^2_{J_y} = (zv_x)^2 \left(\left(\frac{\sigma_{v_x}}{v_x} \right)^2 + \left(\frac{\sigma_z}{z} \right)^2 \right) + (v_z x)^2 \left(\left(\frac{\sigma_{v_z}}{v_z} \right)^2 + \left(\frac{\sigma_x}{x} \right)^2 \right)$$

$$\sigma^2_{J_z} = (xv_y)^2 \left(\left(\frac{\sigma_{v_y}}{v_y} \right)^2 + \left(\frac{\sigma_x}{x} \right)^2 \right) + (v_x y)^2 \left(\left(\frac{\sigma_{v_x}}{v_x} \right)^2 + \left(\frac{\sigma_y}{y} \right)^2 \right)$$

Where σ_A is the error in value A. Assuming that there is no error in the Galactic coordinates for each star, a typical error in J_z for our stars is between 100 and 180 kpc km s^{-1}. The error in J_{Plane} is of roughly the same size. In Fig. 7 the errors are roughly as large as the star symbols, and are therefore not plotted, since they would not affect the analysis.

In Fig. 7 we can see that our stars (along with the rest of the stars from Bobylev et al. 2010) fall in a rather narrow range in J_z. This is hardly surprising, given that they were selected for their very similar V-velocities, which J_z is very sensitive to (c.f. Eq. 3). We can also see that our stars fall right on the edge of the halo, almost right under the stream found by Helmi et al. (1999). The Helmi et al. (1999) stars are distributed all over the sky, but all have pro-grade high-inclination orbits around the Galactic centre. They are seen as a clump in angular momentum space at $\sim 700 < J_z < 1500$ and $J_{plane} \sim 2000$ (see Fig 7). Helmi et al. (1999) compared this stream to simulations and came to the conclusion that its angular momentum is consistent with a dwarf spheroidal galaxy, similar to Fornax, that was accreted by the Milky Way ∼10 Gyrs ago. The stream was later verified by Kepley et al. (2007) who determined that the progenitor galaxy was accreted 6 to 9 Gyrs ago. Kepley et al. (2007) also found a second group of stars on retrograde orbits (indicated in Fig 7) that are probable members of another halo stream.

3.6 HR-Diagrams and Ages

The estimated ages resulting from the isochrone fitting during the abundance analysis (see Table 4) clearly divides our stars into two groups: one young and one old. This is obviously not consistent with our stars being a distinct stellar population, so we constructed two HR-diagrams: one using photometry from the Hipparcos catalogue (ESA 1997) and parallaxes from van Leeuwen (2007) (Fig. 8 and Table 5). We also constructed one HR-diagram using our effective temperatures and surface gravities (Fig. 9).

Starting by looking at Fig. 8 we see that the main group stars align fairly well around the 12.6 Gyrs, [Fe/H]$= -0.72$ isochrone, which is good, since that is close to both the metallicity and the age of the main group. The HR-diagram also confirms that the main group stars are old, and as such seems to indicate that the young age estimates from the abundance analysis in fact are erroneous. We also see why it was impossible to estimate the age of some stars, since they are positioned far down on the main sequence. It

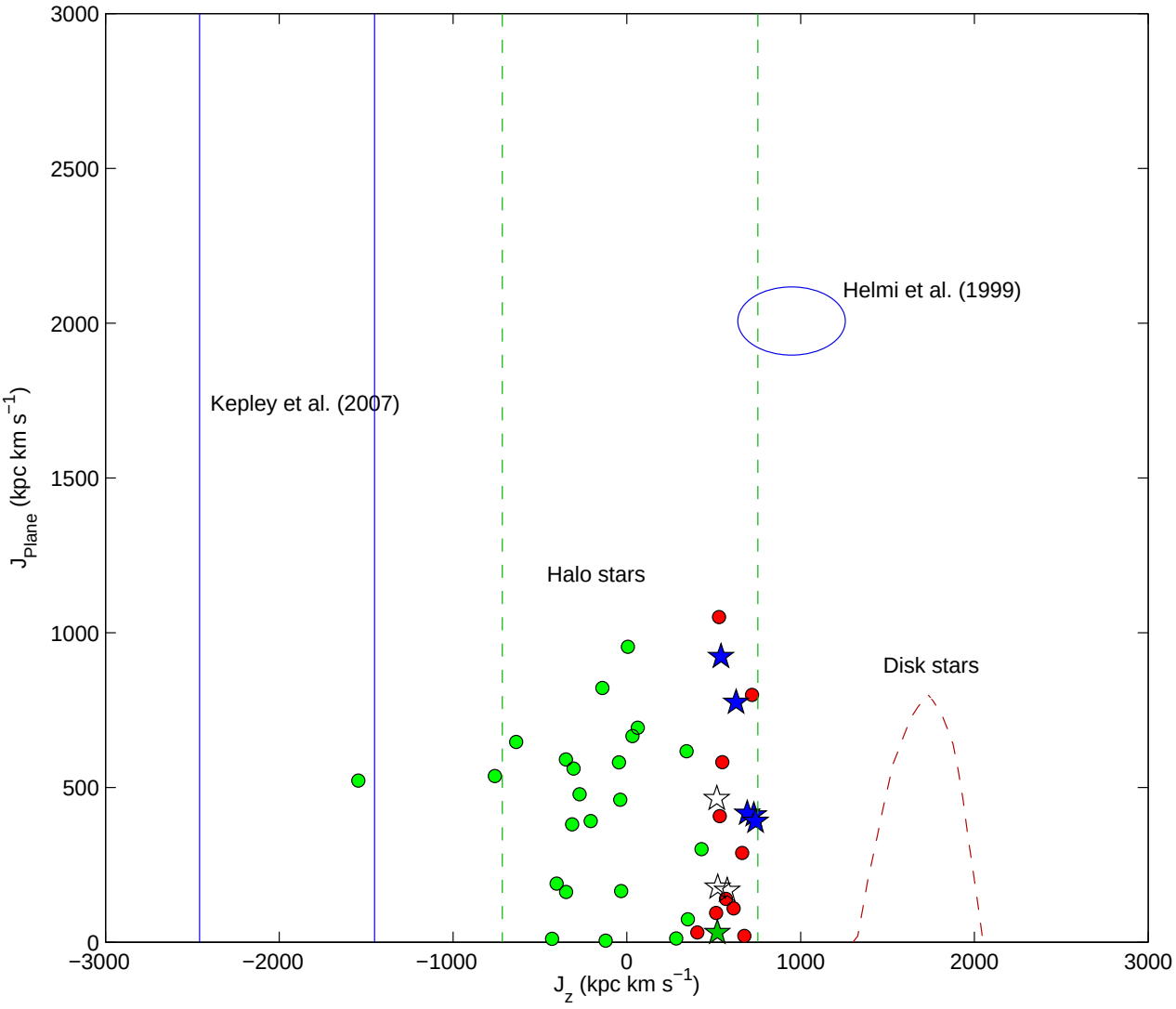

Figure 7: Angular momentum plot of J_{plane} as a function of J_z. Stars mark our stars, empty stars are our stars with metallicity $-0.30 >$[Fe/H]> -0.80, filled blue stars have metallicity $-0.80 >$[Fe/H]> -0.95, and the green filled star has a metallicity [Fe/H]$= -1.58$. Also marked are the rest of the potential member stars of KFR08 from Bobylev et al. (2010) (red circles) and the stars studied in Lagerholm (2010) (green circles). Furthermore, the blue ellipse and the blue lines mark where the stars found by Helmi et al. (1999) and Kepley et al. (2007), respectively, are located. Finally, the general location of halo and disk stars is indicated with green and red dashed lines, respectively.

Table 5: This table lists the photometric data and parallaxes used to make the HR-diagram in Fig. 8 for both our and the Bobylev et al. (2010) stars. The V and $B-V$ magnitudes were taken from the Hipparcos catalogue (ESA 1997) and the parallaxes from the new Hipparcos reduction (van Leeuwen 2007)

Star ID	V (mag)	$B-V$ (mag)	Parallax (mas)
HIP 5336	5.88	0.704	132.38±0.82
HIP 54469	4.68	0.565	9.27±1.29
HIP 58357	2.53	0.860	6.85±0.99
HIP 58708	2.86	0.860	17.52±0.51
HIP 58843	4.98	0.585	14.24±1.33
HIP 60747	5.91	0.706	12.21±1.60
HIP 74033	3.98	0.575	13.91±1.21
HIP 81170	6.34	0.736	22.17±1.35
HIP 87101	4.47	0.672	9.09±1.27
HIP 15495	6.53	0.834	21.67±1.30
HIP 18235	2.64	0.820	15.57±0.57
HIP 19143	7.18	0.964	27.35±1.75
HIP 55988	8.02	1.193	36.50±1.69
HIP 59785	0.79	1.002	8.12±0.45
HIP 64920	0.71	0.981	6.04±0.57
HIP 93269	4.89	0.690	13.93±0.76
HIP 93623	5.69	0.663	16.37±1.47
HIP 96185	4.10	0.595	31.33±0.39
HIP 117702	5.92	0.794	19.84±1.07

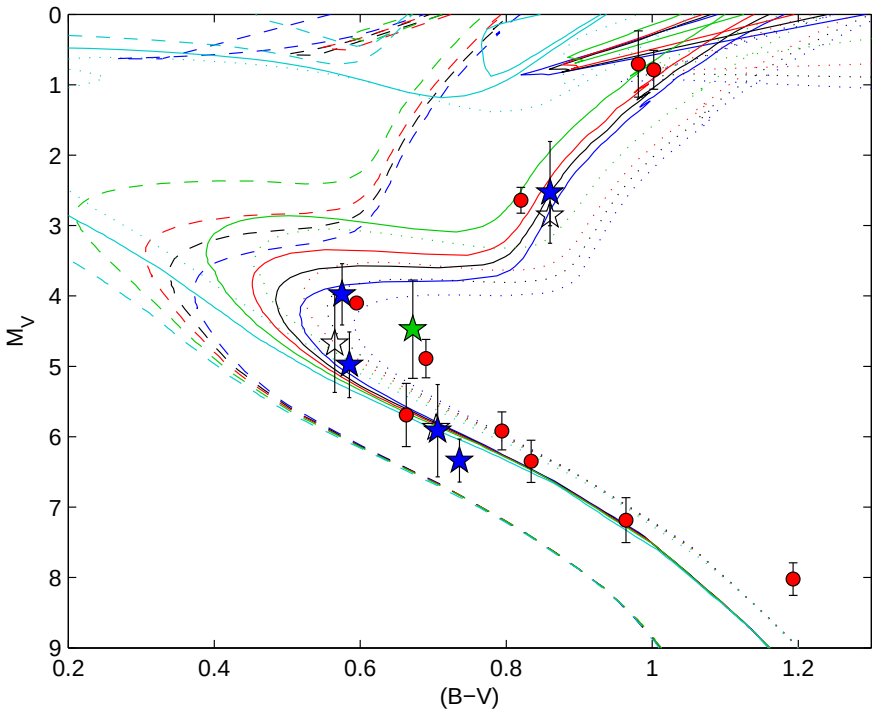

Figure 8: HR diagram with our stars and the rest of the stars from Bobylev et al. (2010). The star symbols are the same as in Fig. 7. Vertical errorbars indicate the error in M_V due to the parallax error. $B-V$ errorbars are as large, or smaller than, the symbols. The lines are isochrones, different line styles represents different metallicities: dashed line is [Fe/H]$= -1.74$, solid line is [Fe/H]$= -0.72$ and dotted line is [Fe/H]$= -0.41$. Furthermore, the different colours represent different ages: blue is 12.6 Gyrs, black is 10.0 Gyrs, red is 9.0 Gyrs, green is 5.0 Gyrs and light blue is 1.0 Gyr. Isochrones from Bertelli et al. (2009).

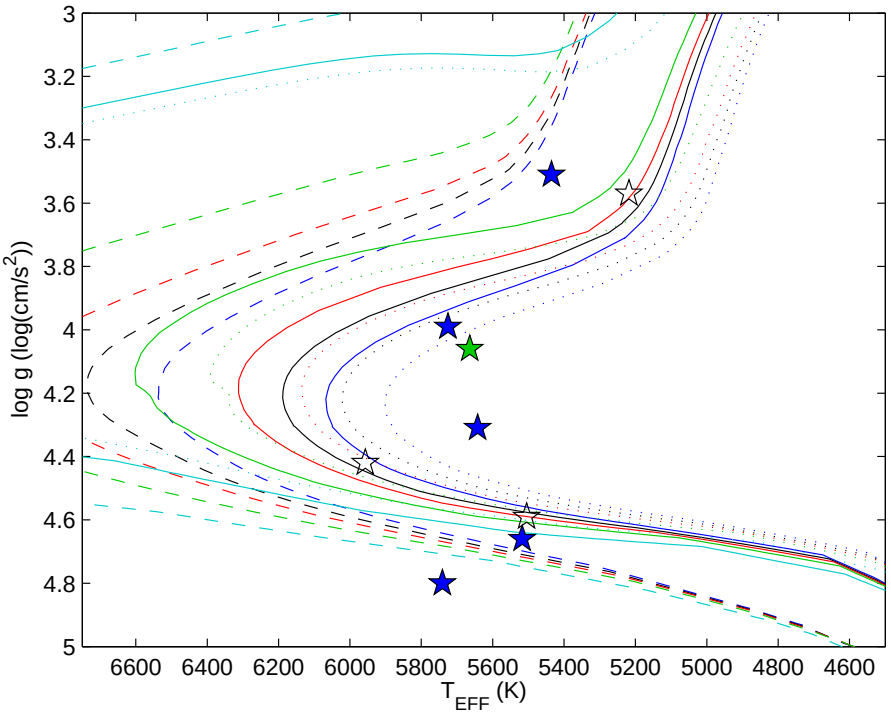

Figure 9: HR diagram using effective temperature and $\log g$ from the abundance analysis. Star symbols and isochrone lines are the same as in Fig. 8

is noteworthy that HIP 87101 (green star in Fig. 8), which is very metal-deficient actually lies closer to the [Fe/H]= -0.07 isochrone (dotted lines) than the [Fe/H]= -1.74 isochrone (dashed lines), which it should lie close to, according to our abundance analysis. This might indicate an error in the magnitudes for HIP 87101, possibly due to it being a binary star, although we have found no evidence for it. If HIP87101 is a binary, then the abundances for it are wrong as well.

If we instead look at Fig. 9 we see that the stars are a lot more spread out in this plot compared to Fig. 8 and that they don't line up with a single isochrone nearly as nicely. HIP 60747 especially seems to lie in a very strange place, indicating that it has metallicity of [Fe/H]< -1.74, while the abundance analysis places it at [Fe/H]= -0.85.

4 Discussion

Looking at our results, we believe that it is quite possible that some of our stars are part of their own moving group (i.e. KFR08), since five of them are quite similar to each other in metallicity, angular momentum and age (if one looks at Fig 8 and not at the abundance analysis age estimates). The similarities are especially prominent with the stars HIP 58357, HIP 58843 and HIP 74033, which all lie very close together in angular momentum space and all have $-0.82 <$ [Fe/H] < -0.91. There are also stars that are significantly deviating in metallicity, especially HIP 58708 and HIP 87101 at [Fe/H]= -0.33 and -1.58, respectively. We believe that this deviation is significant enough to exclude them from membership of KFR08.

Our stars also have strikingly similar J_z values to those of the Helmi et al. (1999) stream. They are probably *not* members of that stream, however, for several reasons: they have a significantly higher metallicity, the Helmi et al. (1999) stream stars all have [Fe/H]< -1.6 dex and our most metal-deficient star, HIP 87101, has [Fe/H] = -1.58 dex. Obviously, HIP 87101 has a metallicity very close to that of the Helmi et al. (1999) stream stars, but it also has a J_{Plane} very close to zero while the Helmi stream stars all have high J_{Plane} values, around 2000 kpc km s^{-1}. The stars other than HIP87101 have quite a bit lower metallicity than the Helmi stream stars. They also have a significantly lower J_{Plane} values than the Helmi stream stars, indicating lower inclination orbits.

4.1 Comparisons With Other Studies

We compare our abundances and angular momenta to the results of Bobylev et al. (2010) obtained in their study. We also compare our results to a study by Lagerholm (2010), which is a study similar to ours, but with a larger scope. They performed abundance analysis on a sample of 23 stars in the halo and studied kinematics of 31 stars (including the aforementioned 23).

Comparing our metallicities to those given in Bobylev et al. (2010) we notice that the stars in the main group at [Fe/H]≈ -0.9 have a little bit lower metallicity than the same stars in Bobylev et al. (2010), where they lie around [Fe/H] ≈ -0.75. Also notable is that our metallicity for HIP 81170 is a bit lower than theirs ([Fe/H]$= -1.26$), which means that their value is more in line with the rest of the stars. Their metallicity for HIP 54469 ([Fe/H]$= -0.72$) is a little lower than ours, however.

If we compare our α-element abundances to those of Lagerholm (2010) (see Fig. 10) we see that both sets of stars are α-enriched, and that we have quite similar spread in our abundances. Our [Mg/Fe] values are a bit higher than theirs in general, though. We do not see our stars split into different groups of [Mg/Fe] and [Si/Fe] above [Fe/H]$= -1.50$ like Lagerholm (2010) observed in their study. Looking at our iron-peak abundances (see Fig. 11), we see that they had the same problem as we have, with their [Cr/Fe] values generally being above zero, albeit less so. The [Ni/Fe] values are more nicely aligned around zero, for both our stars and theirs.

4.2 Final KFR08 Membership Stars

Working under the assumption that KFR08 is a true moving group, then, out of our nine studied stars, five stars (HIP 58357, HIP 58843, HIP 60747, HIP 74033 and HIP 81170, the main group) are very similar in metallicity (see Table 4). Three of these stars (HIP 58357, HIP 58843 and HIP 74033) also have extremely similar angular momenta, while the remaining two have similar J_z, but differ in J_{plane} (See Fig. 7). Regarding age, the main group stars line up nicely along a 12.6 Gyr, [Fe/H]$= -0.72$ isochrone, meaning that they are all of the same age (see Fig. 8). The other stars have a higher metallicity (except for HIP87101, which has a lower metallicity, but a very strange position in the HR-diagram), meaning that their position in the HR-diagram indicates a younger age. We believe these similarities are enough to conclude that the main group are probable members of a possible KFR08

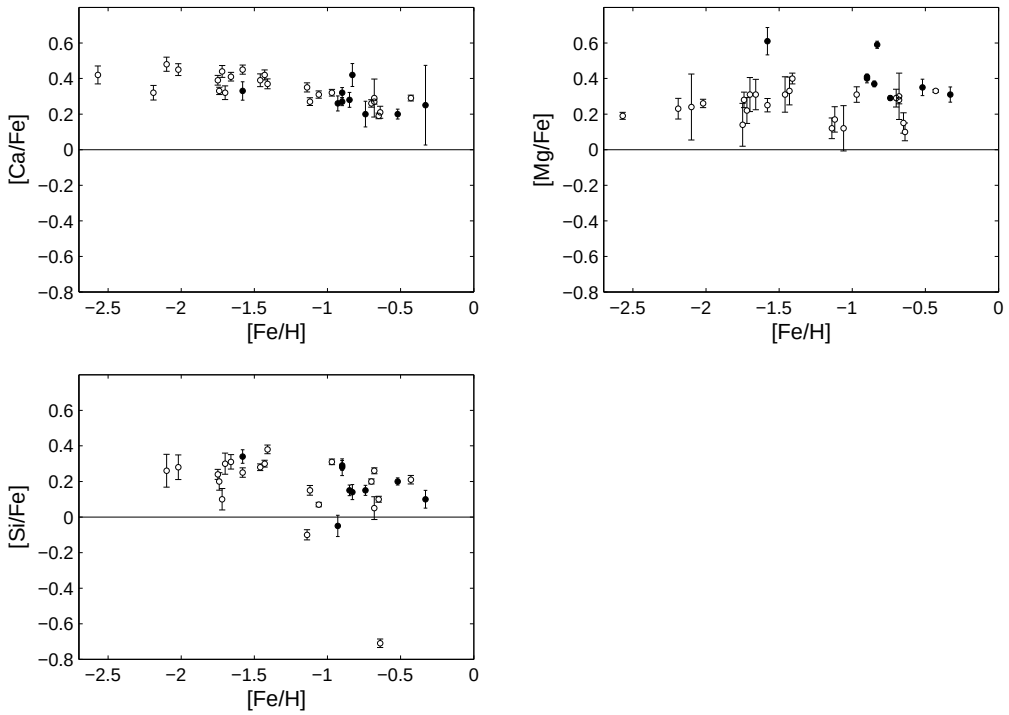

Figure 10: Comparison between our abundance trends of Ca, Mg and Si and those from Lagerholm (2010). Our stars are marked with filled black circles and those from Lagerholm (2010) are marked with empty circles.

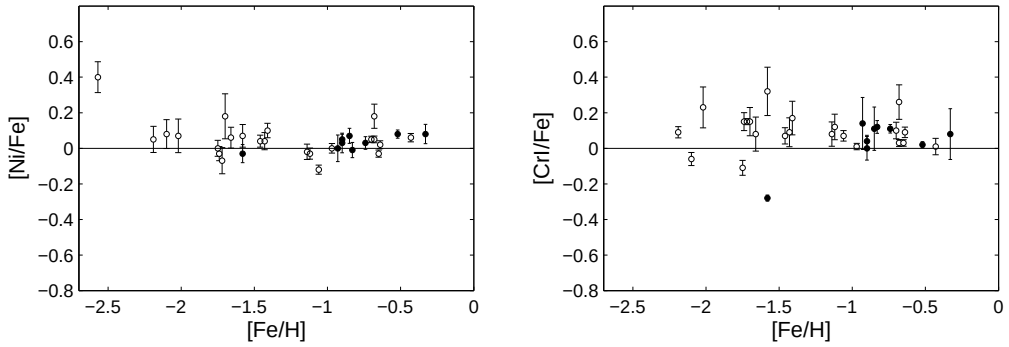

Figure 11: Comparison between our abundance trends of Cr and Ni and those from Lagerholm (2010). Symbols are the same as in Fig. 10

moving group. However, the notion that KFR08 is a stellar stream rather than a moving group (which Bobylev et al. (2010) advocate in their study) should not be discarded since our sample of stars is very small, and thus could possibly just be a small part of a larger KFR08 stream.

4.3 Future Studies

If this study had more time available, the first thing we would do is to remeasure the equivalent widths of all stars. This has been touched upon before, but bears repeating; our errors in the abundances are quite large and could probably be improved by removing lines that give very deviating abundances. This would probably reduce our errors to the levels seen in Lagerholm (2010) and Bensby et al. (2003), since they use the same methodology for deriving the stellar abundances.

Future studies in this field will without doubt benefit greatly from the data that the Gaia mission will provide. All Gaia performance data below are taken from ESA (2011)[1].

Gaia will provide micro-arcsecond parallaxes for roughly a billion stars. This kind of parallaxes would have been invaluable in our study. For example, HIP 58708 has a parallax error of 0.51 arcseconds and a magnitude $V = 6.64$. The same star, measured by Gaia will have a parallax error below 20 micro-arcseconds! Along with the radial velocities Gaia will supply, these parallaxes would be an enormous increase in accuracy that would improve the accuracy of our results significantly.

Perhaps even more fascinating than the high accuracy of Gaia's data is the distances at which it will be able to get this data. In our study, our most distant star lies 146 pc away with an apparent magnitude of 8.35 and an absolute magnitude of 2.53. Gaia would have been able to observe this star (assuming no extinction, and that Gaia could observe this star at 20^{th} magnitude), with smaller parallax errors than what current measurements have, at a distance of over 31 kpc! Of course, in reality, extinction could make this observation very difficult, and almost certainly impossible in the plane of the galaxy.

Interesting is also that the spectroscopic instrument on Gaia will provide element abundances for stars brighter than $\sim 11^{th}$ magnitude ($\sim$ 2 million

[1] http://www.rssd.esa.int/index.php?page=Science_Performance&project=GAIA - last updated: 26^{th} of June 2011, at the time of retrieval.

stars), which will be a incredibly interesting data set too look into to try to find moving groups using metallicity signatures. This data, combined with the kinematic data from radial velocities and proper motions, will make finding new moving groups vastly easier.

References

Bensby, T., Feltzing, S., & Lundström, I. 2003, A&A, 410, 527

Bensby, T., Oey, M. S., Feltzing, S., & Gustafsson, B. 2007, ApJ, 655, L89

Bertelli, G., Nasi, E., Girardi, L., & Marigo, P. 2009, A&A, 508, 355

Binney, J. & Merrifield, M. 1998, Galactic Astronomy, ed. Binney, J. & Merrifield, M.

Bobylev, V. V., Bajkova, A. T., & Mylläri, A. A. 2010, Astronomy Letters, 36, 27

Buser, R. 2000, Science, 287, 69

Churchwell, E., Babler, B. L., Meade, M. R., et al. 2009, PASP, 121, 213

De Silva, G. M., Freeman, K. C., Bland-Hawthorn, J., Asplund, M., & Bessell, M. S. 2007, AJ, 133, 694

Dehnen, W. & Binney, J. J. 1998, MNRAS, 298, 387

Eggen, O. J. 1978, ApJ, 222, 203

ESA. 1997, VizieR Online Data Catalog, 1239, 0

ESA. 2011, GAIA Science Performance

Feltzing, S. & Holmberg, J. 2000, A&A, 357, 153

Freeman, K. & Bland-Hawthorn, J. 2002, ARA&A, 40, 487

Gray, D. F. 1992, The observation and analysis of stellar photospheres., ed. Gray, D. F.

Helmi, A., Navarro, J. F., Meza, A., Steinmetz, M., & Eke, V. R. 2003, ApJ, 592, L25

Helmi, A., White, S. D. M., de Zeeuw, P. T., & Zhao, H. 1999, Nature, 402, 53

Hou, L. G., Han, J. L., & Shi, W. B. 2009, A&A, 499, 473

Jurić, M., Ivezić, Ž., Brooks, A., et al. 2008, ApJ, 673, 864

Kepley, A. A., Morrison, H. L., Helmi, A., et al. 2007, AJ, 134, 1579

Klement, R., Fuchs, B., & Rix, H.-W. 2008, ApJ, 685, 261

Lagerholm, C. 2010, The Disk-Halo Transition and the Search for Stellar Streams - 2010-EXA40

Merrifield, M. R. 2004, in Astronomical Society of the Pacific Conference Series, Vol. 317, Milky Way Surveys: The Structure and Evolution of our Galaxy, ed. D. Clemens, R. Shah, & T. Brainerd, 289

Morrison, H. L., Helmi, A., Sun, J., et al. 2009, ApJ, 694, 130

Smith, G. H. 1983, AJ, 88, 1775

Spitzer, Jr., L. 1958, ApJ, 127, 17

Steinmetz, M., Zwitter, T., Siebert, A., et al. 2006, AJ, 132, 1645

van Leeuwen, F. 2007, A&A, 474, 653

A Elemental Abundances

This appendix lists all elemental abundances for all our stars along with their errors and how many lines were used to calculate them.

Table 6: The Al and BaII abundances for all our stars. Each star has three columns for each element, the first lists the abundance, the second lists the number of lines used to calculate the abundance and the third lists σ, the standard deviation of the abundance.

Star ID	[Al/H]	no. of lines	σ	[BaII/H]	no. of lines	σ
HIP 5336	-0.37	3	0.02	-0.74	3	0.14
HIP 54469	-0.33	4	0.03	-0.24	3	0.02
HIP 58357	-0.37	3	0.12	-1.35	3	0.28
HIP 58708	-0.09	1	-	0.07	2	0.60
HIP 58843	-0.64	3	0.02	-0.65	3	0.13
HIP 60747	-	-	-	-0.70	2	0.10
HIP 74033	-	-	-	-0.73	3	0.17
HIP 81170	-	-	-	-0.84	2	0.13
HIP 87101	-	-	-	-1.08	3	0.25

Table 7: The Cr and CrII abundances for all our stars. Each star has three columns for each element, the first lists the abundance, the second lists the number of lines used to calculate the abundance and the third lists σ, the standard deviation of the abundance.

Star ID	[Cr/H]	no. of lines	σ	[CrII/H]	no. of lines	σ
HIP 5336	-0.63	9	0.06	-0.80	5	0.14
HIP 54469	-0.50	5	0.03	-0.33	5	0.07
HIP 58357	-0.71	9	0.09	-1.09	5	0.17
HIP 58708	-0.25	7	0.36	-0.39	5	0.14
HIP 58843	-0.90	6	0.16	-0.81	4	0.03
HIP 60747	-0.74	5	0.27	-0.61	4	0.23
HIP 74033	-0.86	5	0.07	-0.85	5	0.03
HIP 81170	-0.79	7	0.38	-0.96	3	0.27
HIP 87101	-1.86	1	-	-1.24	1	-

Table 8: The Ca and Mg abundances for all our stars. Each star has three columns for each element, the first lists the abundance, the second lists the number of lines used to calculate the abundance and the third lists σ, the standard deviation of the abundance.

Star ID	[Ca/H]	no. of lines	σ	[Mg/H]	no. of lines	σ
HIP 5336	-0.54	18	0.30	-0.45	1	-
HIP 54469	-0.32	18	0.11	-0.17	4	0.09
HIP 58357	-0.41	18	0.26	-0.24	1	-
HIP 58708	-0.08	12	0.76	-0.02	1	-
HIP 58843	-0.63	18	0.09	-0.50	3	0.04
HIP 60747	-0.57	13	0.14	-0.48	1	-
HIP 74033	-0.58	16	0.11	-0.49	1	-
HIP 81170	-0.67	11	0.11	-	-	-
HIP 87101	-1.25	17	0.20	-0.97	3	0.13

Table 9: The Fe and FeII abundances for all our stars. Each star has three columns for each element, the first lists the abundance, the second lists the number of lines used to calculate the abundance and the third lists σ, the standard deviation of the abundance.

Star ID	[Fe/H]	no. of lines	σ	[FeII/H]	no. of lines	σ
HIP 5336	-0.74	135	0.15	-0.76	16	0.32
HIP 54469	-0.52	151	0.13	-0.35	22	0.10
HIP 58357	-0.83	132	0.23	-1.24	16	0.19
HIP 58708	-0.33	75	0.37	-0.47	9	0.12
HIP 58843	-0.90	147	0.10	-0.74	18	0.23
HIP 60747	-0.85	85	0.15	-0.85	10	0.38
HIP 74033	-0.90	114	0.11	-0.85	19	0.07
HIP 81170	-0.93	82	0.24	-1.12	11	0.44
HIP 87101	-1.58	111	0.18	-1.34	15	0.11

Table 10: The Na and Ni abundances for all our stars. Each star has three columns for each element, the first lists the abundance, the second lists the number of lines used to calculate the abundance and the third lists σ, the standard deviation of the abundance.

Star ID	[Na/H]	no. of lines	σ	[Ni/H]	no. of lines	σ
HIP 5336	-0.71	4	0.06	-0.71	37	0.20
HIP 54469	-0.38	4	0.07	-0.44	40	0.13
HIP 58357	-0.67	4	0.08	-0.84	37	0.23
HIP 58708	-0.15	4	0.05	-0.25	23	0.16
HIP 58843	-0.81	4	0.08	-0.87	37	0.33
HIP 60747	-0.85	4	0.05	-0.78	17	0.16
HIP 74033	-0.76	2	0.02	-0.85	30	0.15
HIP 81170	-1.03	4	0.21	-0.93	17	0.29
HIP 87101	-1.65	2	0.08	-1.61	19	0.21

Table 11: The Ti and TiII abundances for all our stars. Each star has three columns for each element, the first lists the abundance, the second lists the number of lines used to calculate the abundance and the third lists σ, the standard deviation of the abundance.

Star ID	[Ti/H]	no. of lines	σ	[TiII/H]	no. of lines	σ
HIP 5336	-0.29	15	0.20	-0.58	8	0.31
HIP 54469	-0.33	11	0.10	-0.12	7	0.25
HIP 58357	-0.39	13	0.14	-1.10	8	0.32
HIP 58708	0.24	12	0.27	-0.11	6	0.18
HIP 58843	-0.69	10	0.10	-0.59	7	0.21
HIP 60747	-0.40	9	0.19	-0.65	7	0.17
HIP 74033	-0.62	10	0.08	-0.66	8	0.15
HIP 81170	-0.30	9	0.18	-0.83	6	0.07
HIP 87101	-1.28	4	0.05	-1.24	7	0.15

Table 12: The YII and Zn abundances for all our stars. Each star has three columns for each element, the first lists the abundance, the second lists the number of lines used to calculate the abundance and the third lists σ, the standard deviation of the abundance.

Star ID	[YII/H]	no. of lines	σ	[Zn/H]	no. of lines	σ
HIP 5336	-0.81	4	0.28	-1.01	1	-
HIP 54469	-0.22	4	0.08	-0.65	1	-
HIP 58357	-1.47	3	0.33	-1.22	1	-
HIP 58708	-0.25	4	0.31	-	-	-
HIP 58843	-0.98	3	0.16	-	-	-
HIP 60747	-0.64	1	-	-	-	-
HIP 74033	-1.07	3	0.13	-1.08	1	-
HIP 81170	-0.75	4	0.23	-	-	-
HIP 87101	-1.68	3	0.08	-	-	-

Table 13: The Si abundances for all our stars. Each star has three columns for each element, the first lists the abundance, the second lists the number of lines used to calculate the abundance and the third lists σ, the standard deviation of the abundance.

Star ID	[Si/H]	no. of lines	σ
HIP 5336	-0.65	14	0.11
HIP 54469	-0.44	10	0.09
HIP 58357	-0.79	14	0.24
HIP 58708	-0.27	12	0.30
HIP 58843	-0.85	10	0.12
HIP 60747	-0.69	9	0.23
HIP 74033	-0.85	10	0.05
HIP 81170	-0.83	10	0.34
HIP 87101	-1.55	2	0.44